Spin Absorption by *In Situ* Deposited Nanoscale Magnets on Graphene Spin Valves

Walid Amamou,[1] Gordon Stecklein,[2,*] Steven J. Koester,[3] Paul A. Crowell,[2] and Roland K. Kawakami[1,4]

[1] *Program of Materials Science and Engineering, University of California, Riverside, California 92521, USA*
[2] *School of Physics and Astronomy, University of Minnesota, Minneapolis, Minnesota 55455, USA*
[3] *Department of Electrical and Computer Engineering, University of Minnesota, Minneapolis, Minnesota 55455, USA*
[4] *Department of Physics, The Ohio State University, Columbus, Ohio 43210, USA*

(Received 4 April 2018; revised manuscript received 9 July 2018; published 19 October 2018)

An *in situ* measurement of spin transport in a graphene nonlocal spin valve is used to quantify the spin current absorbed by a small (250×750 nm^2) metallic island. The experiment allows for successive depositions of either Fe or Cu without breaking vacuum, so that the thickness of the island is the only parameter that is varied. Furthermore, by measuring the effect of the island using separate contacts for injection and detection, we isolate the effect of spin absorption from any change in the spin injection and detection mechanisms. As inferred from the thickness dependence, the effective spin current $j_e = (2e/\hbar)j_s$ absorbed by Fe is as large as 10^8 A/m^2. The maximum value of j_e is limited by the resistance-area product of the graphene/Fe interface, which is as small as $3\,\Omega\,\mu$m^2. The spin current absorbed by the same thickness of Cu is smaller than that for Fe, as expected given the longer spin-diffusion length and larger spin resistance of Cu compared to Fe. These results allow for a quantitative assessment of the prospects for achieving spin-transfer-torque switching of a nanomagnet using a graphene-based nonlocal spin valve.

DOI: 10.1103/PhysRevApplied.10.044050

I. INTRODUCTION

Graphene is a promising material for lateral-spin transport due to its low spin-orbit coupling and high carrier mobility, leading to long spin-diffusion lengths at room temperature [1,2]. The graphene/ferromagnet (FM) interface has proven to be the bottleneck for achieving long-spin lifetimes and high-spin-injection efficiencies, due to spin absorption by the ferromagnetic contacts [3–13], the possibility of contact-induced spin-relaxation mechanisms other than spin absorption [14], and the challenge of separating these effects from the spin injection and detection efficiencies of the ferromagnet contacts. Understanding spin relaxation and spin absorption at graphene/FM junctions is also important for technological applications such as all-spin logic, in which the magnetization of a nanomagnet is switched by spin-transfer torque when a pure spin current is absorbed [15]. Despite apparent progress [16,17], this goal has been challenging to achieve in graphene, which is why an experiment observing the evolution of the absorbed spin current while varying the thickness of the nanomagnet is valuable.

In this report, we quantify the spin current absorbed by a nanomagnetic island deposited on a nonlocal graphene spin valve. Spin transport measurements are completed *in situ* while growing the Fe island and the results are interpreted using a 2D finite-element model. We determine that the effective spin current absorbed by Fe is as large as $j_e = (2e/\hbar)j_s = 10^8$ A/m^2 and is limited by the resistance-area product of the graphene/Fe interface, which we find to be as low as $3\,\Omega\,\mu$m^2. When the Fe is replaced with Cu, the spin current absorbed by the same thickness is smaller than for Fe, as expected given the longer spin-diffusion length and larger spin resistance of Cu compared to Fe.

II. EXPERIMENT

The experiments are conducted in an ultrahigh vacuum chamber with the ability to perform *in situ* spin-transport measurements between sequential depositions of metallic adatoms. The experiments use multilayer graphene (MLG) spin valves held at cryogenic temperatures (approximately 20 K). For the fabrication of spin-valve devices, MLG flakes are exfoliated onto SiO_2(300 nm)/Si, where the degenerately doped Si is used as a back gate. A single e-beam lithography pattern of bilayer PMMA/methylmethacrylate (MMA) resist

*gordon.stecklein@gmail.com

combined with multi-angle shadow evaporation is utilized to define an SrO tunnel barrier and 60-nm-thick Co electrodes. Details of the device fabrication are provided elsewhere [18]. Subsequently, the spin-valve device is spin coated with PMMA and soft baked at 50 °C for 2 h in order to prevent damaging the SrO/Co electrodes. After the bake, an opening in the PMMA is created for the island deposition using e-beam lithography for patterning and developing in methyl isobutyl ketone (MIBK)/2-propanol (IPA) for 1 m 20 s. Immediately after development, the sample is loaded into the chamber to perform the nonlocal spin-transport measurement and deposit the Fe or Cu island, which is carried out by cryogenic MBE at a pressure below 1×10^{-10} Torr. Unless otherwise noted, the samples are held at 20 K during growth in order to reduce the lateral surface diffusion of adatoms on graphene [19]. A schematic of the device and a SEM image after measurement are shown in Figs. 1(a) and 1(b), and important parameters for each device are provided in Table I. Thermal effusion cells are utilized for the island growth and the growth rate is measured using a quartz-crystal monitor. Typical growth rates are 0.04 Å/min for Fe and 0.2 Å/min for Cu [18]. It is important to note that achieving consistent measurements through many deposition cycles before failure of the device critically depends on the SrO barriers, which have proven to be remarkably robust [18].

The experiment is performed four times, which we refer to as Experiments 1–4. Spin-transport measurements of the MLG spin-valve devices are carried out at 20 K (300 K in Experiment 3) using lock-in detection with an ac injection current of $I = 1$ μA rms at 11 Hz. Initial measurements are conducted at a gate voltage $V_g = 0$ V. Injected spins diffuse throughout the graphene channel and generate the nonlocal voltage V_{NL} indicated in Fig. 1(a). Spin transport is detected by monitoring the nonlocal resistance R_{NL}, defined as $R_{\mathrm{NL}} = V_{\mathrm{NL}}/I$, as a function of an in-plane magnetic field applied along the long axes of the FM electrodes. Figure 1(c) shows data for a representative MLG spin valve (Experiment 1) with MLG of width 2.5 μm and injector-detector electrode spacing of 1.5 μm. The abrupt change in R_{NL}, labeled as ΔR_{NL}, occurs when the injector and detector magnetizations switch between parallel and antiparallel alignments. Notably, ΔR_{NL} quantifies the spin accumulation at the detector. To determine the spin lifetime and diffusion constant for the MLG, we perform nonlocal Hanle-spin precession measurements, in which an out-of-plane magnetic field is ramped while measuring R_{NL}. The Hanle curves for parallel and antiparallel magnetization states are shown in Fig. 1(d). Following a procedure described elsewhere [20], we fit the difference of the Hanle curves and for the example shown obtain a spin lifetime of $\tau_s = 585$ ps, a diffusion constant of $D = 35$ cm^2/s, and a spin injection/detection efficiency $\alpha = 11.3\%$. This fit accounts for spin absorption by the graphene/SrO/Co contacts according to the measured

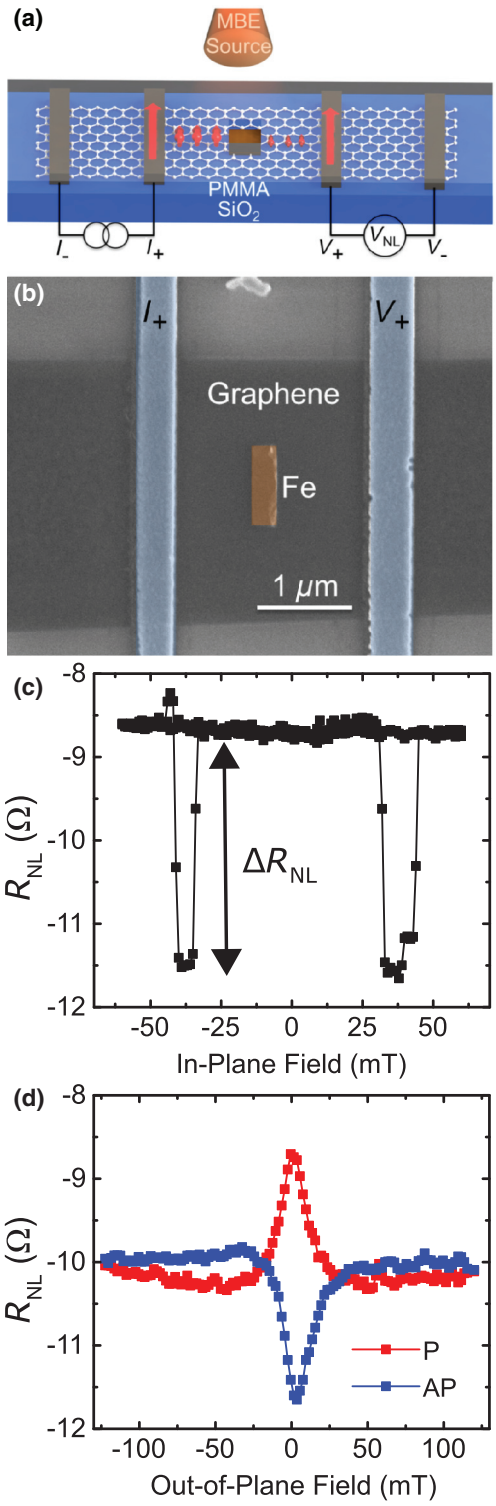

FIG. 1. Graphene nonlocal spin valve island experiment. (a) Device layout and measurement configuration. (b) False-color SEM image after measurement of the device used in Experiment 1. (c) Spin valve measurement taken prior to Fe deposition, indicating spin valve signal size ΔR_{NL}. (d) Nonlocal Hanle measurement taken prior to Fe deposition, with parallel (P) and antiparallel (AP) injector and detector contact magnetization configurations.

TABLE I. Device information and the results of the analysis for all four experiments. The symbols W and d indicate the flake width and injector-detector separation, respectively. The island length refers to the direction perpendicular to the contact magnetization. All values are calculated at the measurement temperature and $V_g = 0$ V prior to depositing the island.

Experiment	1	2	3	4
Island metal(s)	Fe	Fe	Fe	Cu, Fe
W (μm)	2.5	2.7	2.0	1.9
d (μm)	1.5	2.1	2.0	2.2
Island length (nm)	250	200	500	200
R_{sq} (Ω/sq)	1120	393	956	194
ΔR_{NL}^0 (Ω)	2.79	5.84	1.32	0.735
τ_s (ps)	585	736	310	230
D (cm^2/s)	35	370	100	200
α (%)	11.3	11.3	8.0	10

contact resistances, which are typically 2–5 kΩ. The spin-transport properties of the graphene channel are assumed to be constant as the island is deposited.

To investigate the effect of depositing Fe, we measure the spin-transport signal ΔR_{NL} as a function of Fe thickness (t_{Fe}). After each cycle of Fe deposition, we slightly adjust V_g to maintain a constant channel resistance to offset any electrical doping or current-shunting effects. Figure 2(a) shows representative nonlocal magnetoresistance scans at several thicknesses, and Fig. 2(b) summarizes $\Delta R_{NL}(t_{Fe})$. The most important feature of the data is the reduction of ΔR_{NL} as the Fe thickness increases. Most of the signal reduction occurs within the first monolayer of deposition, as can be seen most easily in the inset of Fig. 2(b), which compares the signal with the Fe thickness on a logarithmic scale. The thickness of a monolayer of bcc Fe is $t_{ML} = 1.43$ Å for (001) planes [21]. The rate of decrease of ΔR_{NL} with coverage is much smaller after monolayer completion, although the value of this baseline is also sensitive to the lateral dimensions of the island, as will be discussed below. The final Fe thickness in each experiment is determined by the eventual failure of the device, probably due to the growth of metal on the sidewalls of the resist.

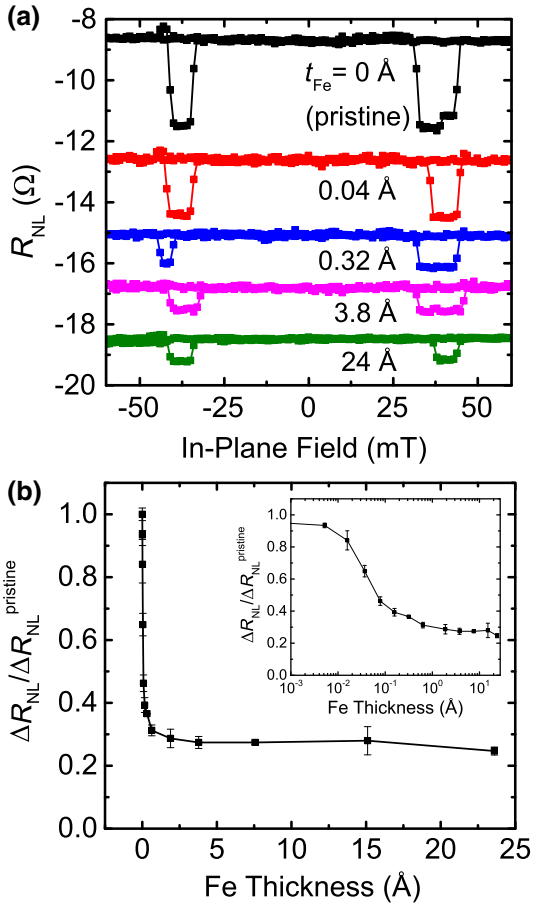

FIG. 2. Effect of depositing the Fe island. (a) In-plane nonlocal magnetoresistance sweeps at different Fe thicknesses. Field sweeps are offset for clarity. (b) Normalized spin valve signal size as a function of Fe thickness, with inset showing the same data using a logarithmic scale for Fe thickness.

III. RESULTS AND DISCUSSION

A. Physical model of spin absorption

In developing a model for the absorption of spin currents in the presence of the island, we must address the observation that ΔR_{NL} decreases on an Fe-thickness scale that is much smaller than the spin-diffusion length in Fe [22], and that a much weaker decrease is observed after monolayer completion. Each of the three experiments in which Fe is directly deposited on graphene shows this behavior, although the fraction of signal that remains varies among the devices, which is due to the geometry and spin-transport properties of the device used for each experiment. To construct the model, we first argue that absorption of a spin current by the island is equivalent to an enhancement Γ in the local spin relaxation rate. In other words,

$$\tau_s^{-1} \rightarrow \tau_s^{-1} + \Gamma, \tag{1}$$

where Γ is a function of the Fe thickness. For the purposes of this paper, we assume that Γ is a scalar quantity, depending only on the magnitude of the spin accumulation. Effects such as anisotropic spin absorption, which would depend on the relative orientations of the spin accumulation and the island magnetization [23], are not included. In this section, we first develop a model for the dependence of Γ on thickness, and then show how the modified spin-relaxation rate can be incorporated into a 2D drift-diffusion calculation of the nonlocal spin signal.

The enhancement factor Γ is proportional to the spin current j_s absorbed by the island. For convenience, we

convert j_s, which has units of spin angular momentum per unit area per unit time, to an effective charge-equivalent spin current $j_e = (2e/\hbar)j_s$. When a spin current is drawn out of the graphene, the local spin splitting of the chemical potential $\Delta\mu = \mu_\uparrow - \mu_\downarrow$ is reduced at the rate Γ such that $\Gamma\Delta\mu = (\partial\mu/\partial n)j_e/e$, where the thermodynamic inverse compressibility $\partial\mu/\partial n$ can be rewritten as $\partial\mu/\partial n = R_{sq}De^2$ by the Einstein relation, where R_{sq} is the graphene square resistance and D is the diffusion constant. In addition, the spin current j_e is related to the spin resistance R_{tot} of the island by $j_e = \Delta\mu/(eR_{tot})$. Therefore, $\Gamma = R_{sq}D/R_{tot}$. We determine the spin current flowing into the island by considering the appropriate spin resistances. Specifically, we represent the island by two spin resistances in series, as shown in Fig. 3. First, longitudinal-spin absorption by the bulk of the island is determined by the island's spin resistance R, which depends on its resistivity ρ, spin diffusion length λ, and thickness t such that $R(t) = \rho\lambda/\tanh(t/\lambda)$ [24,25]. This bulk spin resistance continues to decrease as the island grows thicker until it reaches a thickness greater than its spin diffusion length, at which point the maximum spin current is drawn out of the graphene. This bulk spin current is reduced, however, by an interface resistance R_I, which reaches a constant value as soon as the interface (of area A) is completely formed. We represent the incomplete monolayer by a thickness-dependent area, so that $R_IA(t) = R_IA/\tanh(t/t_{ML})$, where R_IA is the resistance-area product of the graphene/island interface, which we assume fully forms when the island reaches monolayer completion at thickness t_{ML}. Therefore, the thickness dependence of $\Gamma(t)$ due to spin absorption is

$$\Gamma(t) = \frac{R_{sq}D}{\{\rho\lambda/[\tanh(t/\lambda)]\} + \{R_IA/[\tanh(t/t_{ML})]\}}, \quad (2)$$

where the denominator represents the total series resistance shown in Fig. 3. Based on this model and using the known product $R_{sq}D$ for a particular graphene channel, $\Gamma(t)$ can be calculated for given values of ρ, λ, t_{ML}, and R_IA. For example, the effect of the increased spin diffusion length and spin resistance of Cu compared to Fe is shown in Fig. 4. For Fe, we assume $t_{ML} = 1.43$ Å, $\rho_{Fe}(20\text{ K}) = 13\ \mu\Omega$ cm, and $\lambda_{Fe} = 40$ Å [26], for which the spin resistance of the fully formed Fe island is $\rho_{Fe}\lambda_{Fe} = 0.5f\ \Omega\text{m}^2$, as is consistent with results reported elsewhere [22]. For Cu, we assume $t_{ML} = 1.81$ Å, $\rho_{Cu}(20\text{ K}) = 10\ \mu\Omega$ cm (for ultrathin films) [27], and $\lambda_{Cu} = 6000$ Å [28], for which $\rho_{Cu}\lambda_{Cu} = 60f\ \Omega\text{m}^2$. The effect of the Cu island on Γ is observed at larger thicknesses than for Fe because of the longer spin-diffusion length and larger spin resistance of Cu compared to Fe. We note that without any interfacial series resistance, Γ would reach large values (over 1000 ns^{-1}) at very small thicknesses ($t_{Fe} < 0.01$ Å) because of the large mismatch between the graphene and Fe spin resistances. The interface resistance, therefore, plays a critical role.

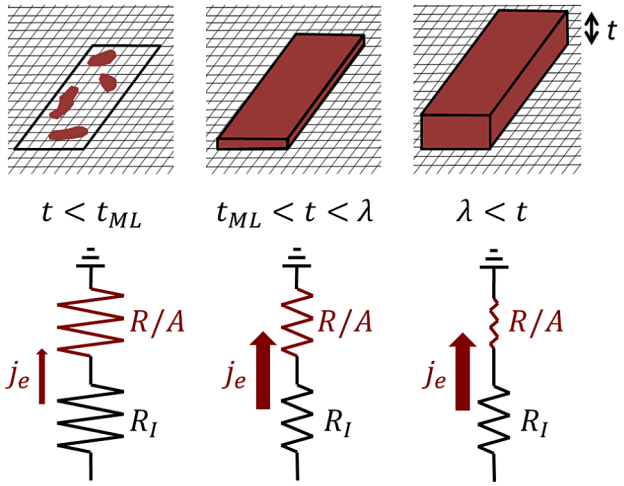

FIG. 3. Physical model of spin absorption as island thickness is varied. As the island thickness t increases, the island's spin resistance per unit area R/A continues to decrease until the island is as thick as its spin-diffusion length λ. As the island is deposited, the interface resistance R_I decreases only until monolayer thickness t_{ML} is reached, at which point the interface is fully formed. The series resistance of these two spin resistances determines the absorbed spin current j_e and thus the effective increase Γ in the local spin-relaxation rate.

Before proceeding, we note that the decrease of the spin signal at small island thicknesses and then the subsequent lack of change in the spin signal when the thickness is further increased would be unexpected in a model in which the bulk-spin-diffusion length is the only parameter. We believe that the model described above is the simplest viable explanation for this behavior, although other microscopic mechanisms are plausible. For example, anisotropic spin absorption may occur prior to depositing a complete monolayer [23,29], or the growth of the island on graphene may not proceed as proposed here despite the agreement observed between our data and the model shown below. We emphasize, however, that it is essentially impossible to distinguish among different microscopic absorption mechanisms using only nonlocal spin valve (NLSV) and Hanle measurements, and we believe the effective relaxation rate as used here is an appropriate description regardless of the mechanism.

B. Finite-element model

The next step is to determine ΔR_{NL} for a given thickness once $\Gamma(t)$ is known. To accomplish this, we perform a 2D finite-element simulation to model the spin accumulation throughout the graphene channel as spins are absorbed by the island. A 2D environment composed of 25×25 nm^2 cells is used to model the spin accumulation $\vec{S}(x,y)$ throughout the graphene channel, where $\vec{S}$

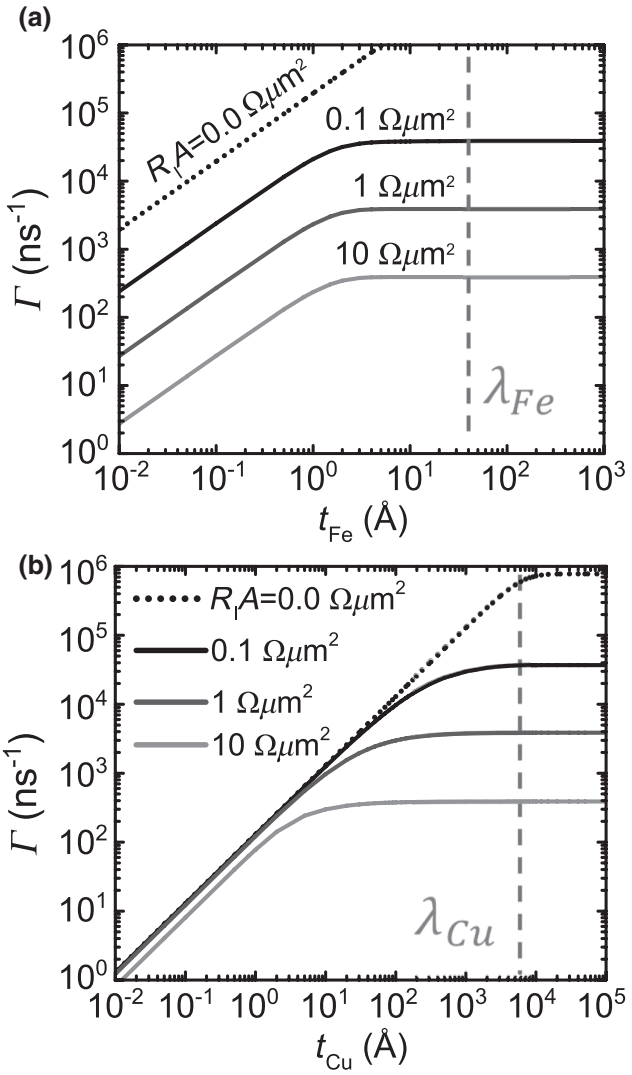

FIG. 4. Contrast between the theoretical thickness dependence $\Gamma(t)$ for (a) Experiment 1, which uses Fe, and (b) Experiment 4, which uses Cu. In each case, different curves indicate the effect of varying the additional interface resistance-area product R_IA. The curves shown here assume $\lambda_{Fe} = 40$ Å, $\lambda_{Cu} = 6000$ Å, and $R_{sq}D = 39$ kΩ cm^2/s, where the latter matches both Experiments 1 and 4. The x axis of the lower plot includes two additional orders of magnitude.

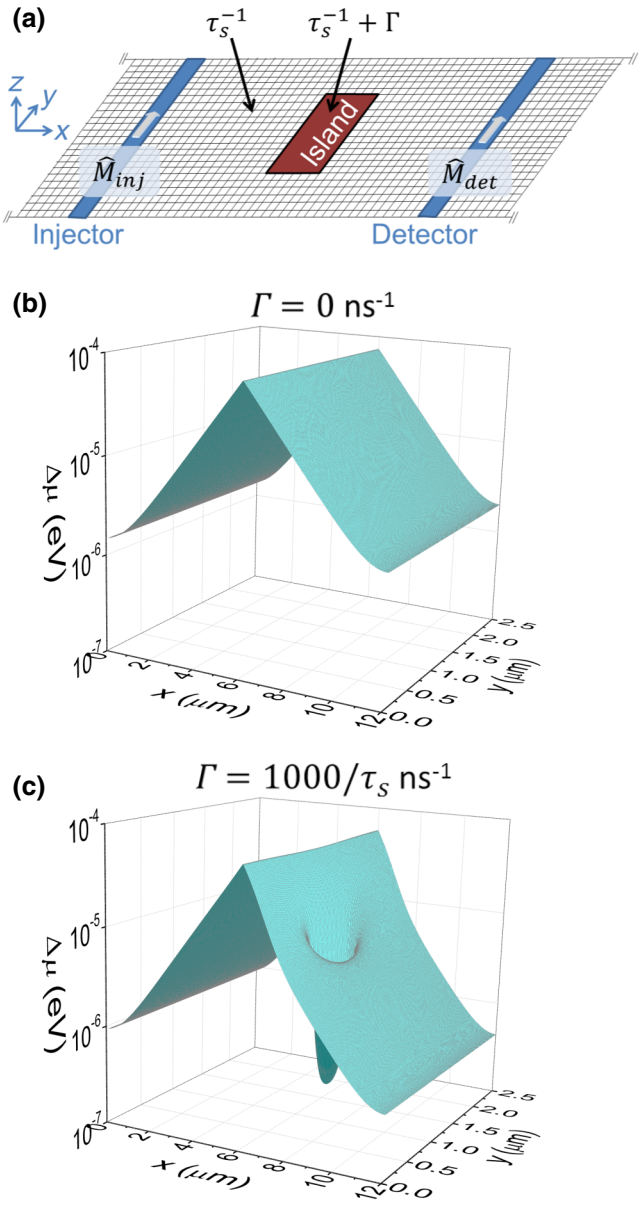

FIG. 5. Finite-element model. (a) Spatially resolved model with additional spin relaxation rate Γ under the island (not to scale). (b) Steady-state solution corresponding to Experiment 1 for $\Gamma = 0$ and (c) $\Gamma = 1000/\tau_s = 1710$ ns^{-1}. This model is used to calculate how the spin valve signal size ΔR_{NL}, which is calculated from $\Delta\mu$ at the detector, depends on the increase Γ in spin relaxation under the island.

is the spin polarization associated with the electrochemical potential splitting $\Delta\mu = \mu_\uparrow - \mu_\downarrow$ for spins oriented along each of the three cardinal directions ($i = x, y, z$). The grid is represented schematically in Fig 5(a). A forward Euler step algorithm with Neumann boundary conditions is used to evolve the distributed spin accumulation until steady state in accordance with spin diffusion, precession, and relaxation [30,31],

$$\frac{\partial \vec{S}}{\partial t} = D\nabla^2\vec{S} - \gamma\vec{B}\times\vec{S} - \frac{\vec{S}}{\tau_s} + \dot{\vec{S}}_0(x,y) = 0, \quad (3)$$

where $\gamma = 1.76\times10^{-2}$ Oe^{-1} ns^{-1} is the gyromagnetic ratio, $\vec{B}$ is the applied magnetic field, and $\dot{\vec{S}}_0(x,y) = 2\alpha\hat{M}_{inj}j_{inj}(\partial\mu/\partial n)/e$ is the rate of spin injection. The spin-injection rate, which is nonzero only under the injector contact, is calculated from the fitted value of α, the injected charge-current density j_{inj}, and $\partial\mu/\partial n = R_{sq}De^2$. Spin absorption into the Co contacts is incorporated into the model as a local increase $\tau_c^{-1} = R_{sq}D/(R_CA)$ in the

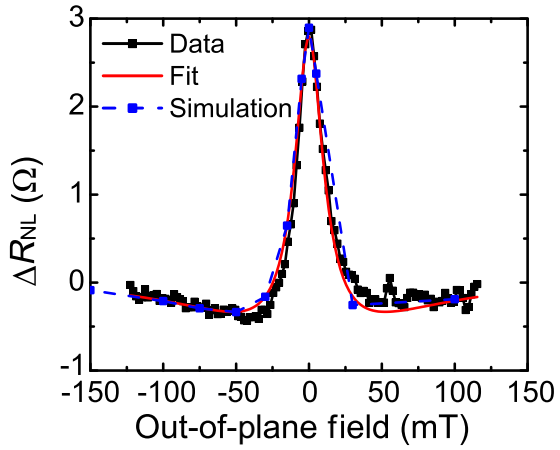

FIG. 6. Comparison of the nonlocal Hanle data taken prior to island deposition to the analytical fit and finite-element model for Experiment 1.

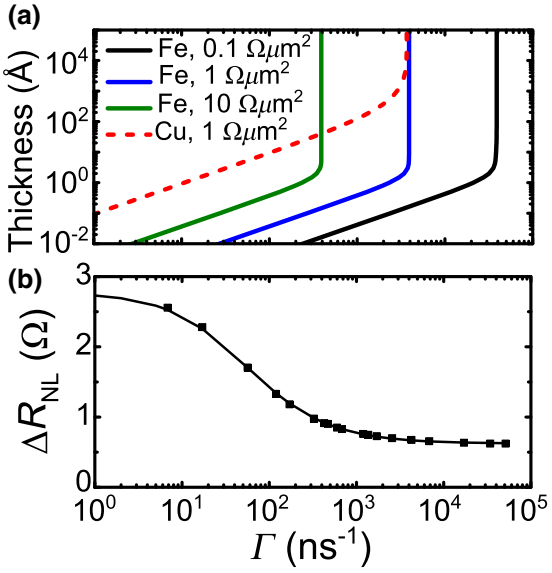

FIG. 7. Analysis and modeling of the experiment. (a) Theoretical relationship between island thickness and additional spin-relaxation rate Γ, for either an Fe or Cu island and for various values of the graphene/metal interface resistance-area product R_IA. These theoretical curves assume spin-diffusion lengths and monolayer thicknesses of $\lambda_{Fe} = 4$ nm and $t_{ML} = 1.43$ Å for Fe and $\lambda_{Cu} = 6000$ Å and $t_{ML} = 1.81$ Å for Cu. (b) Sensitivity of the spin valve signal size ΔR_{NL} to the additional spin-relaxation rate for Experiment 1 determined by the finite-element model. Results of the model are shown as points and a smooth interpolation of these points is shown as a solid curve.

spin-relaxation rate for cells under the Co, where R_C is the measured contact resistance and A is the contact area. The spin absorption into the island is accounted for by increasing the spin-relaxation rate in cells underneath the island by Γ. The simulation is used to determine the component $S_y = \vec{S} \cdot \hat{M}_{det}$ of the spin accumulation parallel to the detector magnetization, from which the spin valve signal size is calculated as $(\Delta R_{NL})_{model} = \alpha \langle S_y \rangle_{det}/I$, where I is the injection charge current and $\langle S_y \rangle_{det}$ is the average of S_y in the cells underneath the detector contact. Examples of $S_y(x, y)$ for $\Gamma = 0$ and 1000 ns^{-1} are shown in Figs. 5(b) and 5(c). As anticipated, the spin accumulation under the island is greatly reduced as Γ increases. Although this suppression is not observed directly, the "sinking" of spin current into the island leads to the decrease of the spin accumulation at the detector [at the right side of each panel in Figs. 5(b) and 5(c)]. The model is verified by confirming that, for $\Gamma = 0$, the out-of-plane magnetic field dependence of ΔR_{NL} is consistent with the nonlocal Hanle data measured prior to metal deposition, as shown for Experiment 1 in Fig. 6.

With this model, we now determine the sensitivity curve $\Delta R_{NL}(\Gamma)$, which describes how the spin accumulation under the detector is affected by an additional spin-relaxation rate under the island, including the effect of spins flowing through side channels around the island. By interpolating between results for many values of Γ, the sensitivity curve $\Delta R_{NL}(\Gamma)$ is calculated for a particular interface resistance-area product R_IA. We find that most variation in ΔR_{NL} occurs when the additional spin-relaxation rate is in the range $\Gamma = 1 - 1000$ ns^{-1}. Any further increase in Γ has little effect on ΔR_{NL} because the effective spin lifetime under the island is already negligibly small. Figure 7(a) shows the relationship between thickness and Γ for various choices of R_IA for Fe and one case for Cu, and Fig. 7(b) shows ΔR_{NL} as a function of Γ. This analysis is completed for each experiment, because the exact sensitivity $\Delta R_{NL}(\Gamma)$ depends on the geometry and spin-transport parameters of each graphene channel. Results for Experiments 2–4 are shown in Fig. 8. Comparison with experiment is achieved by combining $\Gamma(t)$ with $\Delta R_{NL}(\Gamma)$, resulting in $\Delta R_{NL}(t)$. Fitting proceeds by making adjustments in R_IA until the calculated curve $\Delta R_{NL}(t)$ agrees with experiment. The best-fit values of R_IA, which will be discussed further below, are included in Table II.

C. Calculation of the absorbed spin current

We fit the measured thickness dependence $\Delta R_{NL}(t_{Fe})$ to the spin-absorption model using R_IA as the sole fitting parameter. The theoretical thickness dependence $\Gamma(t_{Fe})$ is combined with the sensitivity curve $\Delta R_{NL}(\Gamma)$ to determine $\Delta R_{NL}(t_{Fe})$ for a given value of R_IA. By comparing many such curves with the measured thickness dependence, we find the best-fit value of R_IA. The data and fits for Experiments 1–3 are shown in Fig. 9(a), where the experiments encompass various geometries, Fe-deposition temperatures, and spin-transport properties. In all cases, we fit the data to the spin-absorption model assuming $\lambda_{Fe} = 4$ nm and $t_{ML} = 1.43$ Å.

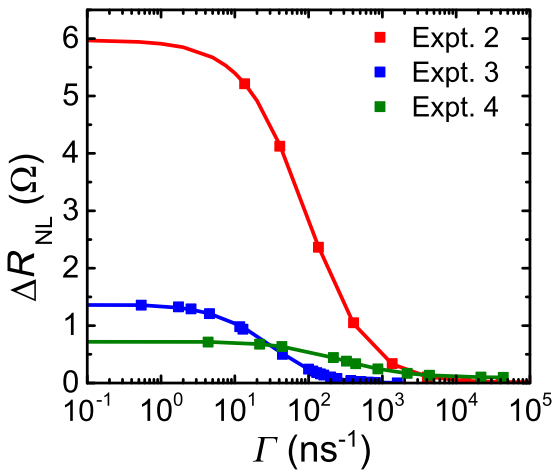

FIG. 8. Sensitivity curves for Experiments 2–4 determined by simulation. These curves quantify how the introduction of additional spin relaxation rate Γ under the island affects the spin signal ΔR_{NL}.

Using the best-fit value of $R_I A$, the spin current absorbed by the island in the limit $t \gg \lambda$ is

$$j_e = \frac{\Delta\mu/e}{\rho\lambda + R_I A} \approx \frac{I\Delta R^0_{\mathrm{NL}} \exp[d/(2\lambda_g)]}{\alpha(\rho\lambda + R_I A)}, \qquad (4)$$

where ΔR^0_{NL} is the spin signal measured prior to depositing the island and the factor $\exp[d/(2\lambda_g)]$ is used to estimate the spin accumulation under the island from the injector-detector separation d and the graphene spin diffusion length $\lambda_g = \sqrt{D\tau_s}$.

For each experiment, the best-fit results for $R_I A$ and the corresponding spin current j_e are shown in Table II. We find $R_I A = 3\ \Omega\mu\mathrm{m}^2$, from which we calculate that the absorbed spin current is as large as $j_e = 10^8\ \mathrm{A/m}^2$. We discuss the physical significance of the extracted values of $R_I A$ in more detail below. Although it is surprising that ΔR_{NL} decays quickly at small Fe thicknesses and then changes little with additional Fe thickness, this behavior is consistent with the assumption that $\lambda_{\mathrm{Fe}} = 4$ nm. As the island is grown, its spin resistance decreases, but the absorbed spin current is ultimately limited by the series resistance of the interface. The local effective spin-relaxation rate, therefore, increases with thickness and then saturates because of the completion of the graphene/Fe interface. The variation in ΔR_{NL} with thickness is explained by the completion of the interface at low thicknesses and the efficiency with which the spin-absorption effect reduces the measured spin accumulation.

To put the calculated spin currents in context, switching the island by antidamping from longitudinal spin absorption is predicted to require an effective spin current of $j_e > (2e/\hbar)\alpha_d t M_s(H_k + H + 2\pi M_s)$, where α_d is the Gilbert damping constant, t is the island thickness, M_s is the island's magnetization, H_k is the easy-axis anisotropy field, and H is the strength of an external magnetic field applied antiparallel to the initial magnetization direction [32,33]. For the island materials used here, an order-of-magnitude estimate of the critical spin current required for field-unassisted ($H = 0$) switching is $j_e = 10^{10}\ \mathrm{A/m}^2$ for a thickness $t = 1$ nm, $\alpha_d = 0.01$, and $H_k = 100$ Oe. We conclude that due to the interface resistance, which we argue below approaches the limiting minimum value expected, the spin currents in our devices are significantly smaller than what would be required to produce switching.

D. Comparison of Cu and Fe islands

In Experiment 4, the process is repeated with a Cu island instead of Fe, where Cu is chosen because it has a longer spin-diffusion length than Fe, is nonmagnetic, has a weak chemical interaction with graphene, and has low spin-orbit coupling. In prior studies, the deposition of Au on a graphene spin valve has been shown to unexpectedly increase the spin signal [34], although this result is not understood. We deposit the Cu island and monitor the spin signal ΔR_{NL} as a function of Cu thickness t_{Cu}. The result of Experiment 4, which is shown in Fig. 9(b), confirms that the decrease in $\Delta R_{\mathrm{NL}}(t_{\mathrm{Cu}})$ occurs over a larger thickness range than for Fe, as expected due to the longer spin-diffusion length and larger spin resistance of Cu.

As with the Fe-island devices, the thickness dependence $\Delta R_{\mathrm{NL}}(t_{\mathrm{Cu}})$ is fit to the spin-absorption model. We find that

TABLE II. Results of fitting the Fe-thickness dependence of ΔR_{NL} to the spin-absorption model. Experiment number, growth temperature, island width (in the direction parallel to the contact magnetization, as a percentage of the channel width), charge injection current I used for the measurement, product of the graphene resistance per square R_{sq} and the diffusion constant D fit from nonlocal Hanle data, best-fit interface resistance-area product $R_I A$, and spin current j_e absorbed by the Fe in the limit $t_{\mathrm{Fe}} \gg \lambda_{\mathrm{Fe}}$ are indicated.

Experiment	Temperature (K)	Island width (% of channel width)	I (μA)	$R_{\mathrm{sq}}D$ (kΩ cm^2/s)	$R_I A$ ($\Omega\,\mu\mathrm{m}^2$)	j_e into Fe (A/m^2)
1	20	30	1	39.1	2.8	1.5×10^7
2	20	85	5	146	3.1	1.0×10^8
3	300	90	1	95.6	12	2.4×10^6
4 (Fe on Cu)	20	32	5	38.9	gr/Cu: 4.8 Cu/Fe: 3.2	1.6×10^6

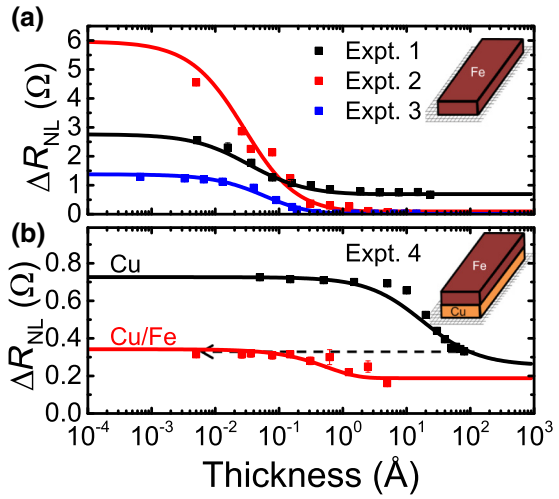

FIG. 9. Fits to the spin absorption model. (a) Measurements of $\Delta R_{NL}(t_{Fe})$ for three different experiments, each fit to the spin-absorption model. (b) Data and fits to the spin-absorption model when Cu is deposited instead of Fe (black), and when Fe is deposited after depositing the Cu interlayer (red). The dashed black arrow indicates the measurement sequence. Results of the fits, including the graphene/metal interface resistance-area product and the calculated spin current, are shown in Table II.

$R_I A = 4.8\ \Omega\mu\text{m}^2$. After depositing 80 Å of Cu, we calculate that $\Gamma_{Cu} = 418\ \text{ns}^{-1}$. In contrast, based on Experiment 1, the effective spin-relaxation rate induced by Fe of the same thickness is three times larger than that for Cu. We conclude that the spin-absorption effect of Cu is smaller than Fe, as expected.

To determine the spin absorption by Fe across a nonmagnetic spacer, the deposition of Cu is halted after 80 Å and Fe deposition is started. The result is also shown in Fig. 9(b), where the data are again fit to the spin-absorption model. In this case, the total additional spin-relaxation rate is $\Gamma = \Gamma_{Cu} + \Gamma_{Fe}(t_{Fe})$, where only the latter term increases with Fe thickness. We find a similar thickness dependence for Fe after Cu as compared to Fe directly on graphene, which is consistent with Fe absorbing a similar spin current in the graphene/Cu/Fe experiment as compared to the graphene/Fe experiments.

E. Fundamental limit of the graphene/metal interface resistance-area product

Finally, we discuss the physical significance of the extracted values for the interface resistance-area product. In the analysis presented above, the fitted values of the graphene/metal interface resistance-area product are approximately 10^3 times larger than either the Fe or Cu spin resistances. To understand the source of this interface resistance, we calculate the theoretical minimum resistance-area product $(R_I A)_{thy}$ of a graphene/metal interface from the number of available modes by $(R_I A)_{thy} = h/(4e^2 n)$, where n is the 2D graphene carrier concentration [35]. For $n = 10^{12}\ \text{cm}^{-2}$, which is the approximate value at the gate voltages used, $(R_I A)_{thy} = 0.6\ \Omega\mu\text{m}^2$. We conclude that the values for the interface resistance-area product that we measure are within an order of magnitude of the theoretical minimum.

Given the low temperature growth of the island by MBE, it is perhaps not surprising that the interfacial resistances are as small as those inferred from the model, with variations that reflect the degree of contamination before growth. We emphasize, however, that we cannot measure $R_I A$ values this small directly in the spin valve device geometry. It is, therefore, possible that the actual $R_I A$ product is *larger* than inferred from our model and that some other mechanism, such as proximity-induced magnetism [36–38] or enhanced spin-orbit coupling [39] at the graphene/metal interface, is leading to a larger interfacial-spin-relaxation rate. Our measurement cannot distinguish between interfacial spin relaxation in the presence of a larger $R_I A$ product and spin absorption. However, we emphasize that the experimental data can be interpreted purely in terms of spin absorption and that we observe no concrete evidence of interfacial spin relaxation. The model we introduce here places an upper bound on the maximum spin current absorbed by the island. The most practical option available for enhancing this value is increasing the spin accumulation in the channel, which will require further optimization of the injection contacts.

IV. CONCLUSION

In conclusion, an *in situ* measurement of nonlocal spin transport is used to quantify the spin current absorbed by a small Fe island on a graphene surface. The Fe thickness dependence is interpreted using a 2D numerical simulation. We find that the data are consistent with a spin-absorption model. Fitting the data to this model shows that the effective spin current absorbed by Fe can be as large as $10^8\ \text{A/m}^2$ for an excitation current $I = 5\ \mu\text{A}$, and this absorbed spin current is limited by an interface resistance-area product of $3\ \Omega\,\mu\text{m}^2$, which is nearing the theoretical minimum for a few-layer graphene/metal interface. A similar *in situ* study of a graphene/Cu/Fe junction is analyzed using the same model, where the effect of Cu is consistent with its longer spin-diffusion length compared to Fe. Given the low resistance-area products achieved and the resulting bound on the absorbed spin current, these results suggest that new approaches will need to be considered – such as increasing the excitation current beyond tens of microamps – in order to achieve the goal of nonlocal spin-transfer torque switching in few-layer graphene, for which effective spin current densities of order $10^{10}\ \text{A/m}^2$ would be required.

ACKNOWLEDGMENTS

We thank Serol Turkyilmaz for his contributions to the development of the experiment. This work was supported by C-SPIN, a SRC STARnet center sponsored by MARCO and DARPA.

W.A. and G.S. contributed equally to this work.

[1] W. Han, R. K. Kawakami, M. Gmitra, and J. Fabian, Graphene spintronics, Nat. Nanotechnol. **9**, 794 (2014).

[2] N. Tombros, C. Jozsa, M. Popinciuc, H. T. Jonkman, and B. J. van Wees, Electronic spin transport and spin precession in single graphene layers at room temperature, Nature (London) **448**, 571 (2007).

[3] S. Takahashi and S. Maekawa, Spin injection and detection in magnetic nanostructures, Phys. Rev. B **67**, 052409 (2003).

[4] A. Fert and H. Jaffrès, Conditions for efficient spin injection from a ferromagnetic metal into a semiconductor, Phys. Rev. B **64**, 184420 (2001).

[5] B. Dlubak, P. Seneor, A. Anane, C. Barraud, C. Deranlot, D. Deneuve, B. Servet, R. Mattana, F. Petroff, and A. Fert, Are Al_2O_3 and MgO tunnel barriers suitable for spin injection in graphene?, Appl. Phys. Lett. **97**, 092502 (2010).

[6] M. Popinciuc, C. Józsa, P. J. Zomer, N. Tombros, A. Veligura, H. T. Jonkman, and B. J. van Wees, Electronic spin transport in graphene field-effect transistors, Phys. Rev. B **80**, 214427 (2009).

[7] C. Józsa, T. Maassen, M. Popinciuc, P. J. Zomer, A. Veligura, H. T. Jonkman, and B. J. van Wees, Linear scaling between momentum and spin scattering in graphene, Phys. Rev. B **80**, 241403 (2009).

[8] P. J. Zomer, M. H. D. Guimarães, N. Tombros, and B. J. vanWees, Long-distance spin transport in high-mobility graphene on hexagonal boron nitride, Phys. Rev. B **86**, 161416 (2012).

[9] W. Han, K. Pi, K. M. McCreary, Y. Li, J. J. I. Wong, A. G. Swartz, and R. K. Kawakami, Tunneling Spin Injection into Single Layer Graphene, Phys. Rev. Lett. **105**, 167202 (2010).

[10] W. Han and R. K. Kawakami, Spin Relaxation in Single-Layer and Bilayer Graphene, Phys. Rev. Lett. **107**, 047207 (2011).

[11] E. Sosenko, H. Wei, and V. Aji, Effect of contacts on spin lifetime measurements in graphene, Phys. Rev. B **89**, 245436 (2014).

[12] F. Volmer, M. Drögeler, E. Maynicke, N. von den Driesch, M. L. Boschen, G. Güntherodt, and B. Beschoten, Role of MgO barriers for spin and charge transport in Co/MgO/graphene nonlocal spin-valve devices, Phys. Rev. B **88**, 161405 (2013).

[13] F. Volmer, M. Drögeler, E. Maynicke, N. von den Driesch, M. L. Boschen, G. Güntherodt, C. Stampfer, and B. Beschoten, Suppression of contact-induced spin dephasing in graphene/MgO/Co spin-valve devices by successive oxygen treatments, Phys. Rev. B **90**, 165403 (2014).

[14] W. Amamou, Z. Lin, J. van Baren, S. Turkyilmaz, J. Shi, and R. K. Kawakami, Contact induced spin relaxation in graphene spin valves with Al_2O_3 and MgO tunnel barriers, APL Mater. **4**, 032503 (2016).

[15] T. Kimura, Y. Otani, and J. Hamrle, Switching Magnetization of a Nanoscale Ferromagnetic Particle Using Nonlocal Spin Injection, Phys. Rev. Lett. **96**, 037201 (2006).

[16] C.-C. Lin, A. V. Penumatcha, Y. Gao, V. Q. Diep, J. Appenzeller, and Z. Chen, Spin transfer torque in a graphene lateral spin valve assisted by an external magnetic field, Nano Lett. **13**, 5177 (2013).

[17] C.-C. Lin, Y. Gao, A. V. Penumatcha, V. Q. Diep, J. Appenzeller, and Z. Chen, Improvement of spin transfer torque in asymmetric graphene devices, ACS Nano **8**, 3807 (2014).

[18] S. Singh, J. Katoch, T. Zhu, R. J. Wu, A. S. Ahmed, W. Amamou, D. Wang, K. A. Mkhoyan, and R. K. Kawakami, Strontium oxide tunnel barriers for high quality spin transport and large spin accumulation in graphene, Nano Lett. **17**, 7578 (2017).

[19] B. Canto, C. P. Gouvea, B. S. Archanjo, J. E. Schmidt, and D. L. Baptista, On the structural and chemical characteristics of Co/Al_2O_3/graphene interfaces for graphene spintronic devices, Sci. Rep. **5**, 14332 (2015).

[20] G. Stecklein, P. A. Crowell, J. Li, Y. Anugrah, Q. Su, and S. J. Koester, Contact-Induced Spin Relaxation in Graphene Nonlocal Spin Valves, Phys. Rev. Appl. **6**, 054015 (2016).

[21] C. Martínez Boubeta, C. Clavero, J. M. García-Martín, G. Armelles, A. Cebollada, Ll. Balcells, J. L. Menéndez, F. Peiró, A. Cornet, and M. F. Toney, Coverage effects on the magnetism of Fe/MgO(001) ultrathin films, Phys. Rev. B **71**, 014407 (2005).

[22] J. Bass and W. Pratt, Spin-diffusion lengths in metals and alloys, and spin-flipping at metal/metal interfaces: an experimentalist's critical review, J. Phys.: Condens. Matter **19**, 183201 (2007).

[23] H. Idzuchi, Y. Fukuma, S. Takahashi, S. Maekawa, and Y. Otani, Effect of anisotropic spin absorption on the Hanle effect in lateral spin valves, Phys. Rev. B **89**, 081308(R) (2014).

[24] T. Valet and A. Fert, Theory of the perpendicular magnetoresistance in magnetic multilayers, Phys. Rev. B **48**, 7099 (1993).

[25] S. Manipatruni, D. E. Nikonov, and I. A. Young, Modeling and design of spintronic integrated circuits, IEEE Trans. Circuits Syst. I Regul. Pap. **59**, 2801 (2012).

[26] L. O'Brien, D. Spivak, N. Krueger, T. A. Peterson, M. J. Erickson, B. Bolon, C. C. Geppert, C. Leighton, and P. A. Crowell, Observation and modelling of ferromagnetic contact-induced spin relaxation in Hanle spin precession measurements, Phys. Rev. B **94**, 094431 (2016).

[27] Y. P. Timalsina, A. Horning, R. F. Spivey, K. M. Lewis, T.-S. Kuan, G.-C. Wang, and T.-M. Lu, Effects of nanoscale surface roughness on the resistivity of ultrathin epitaxial copper films, Nanotechnology **26**, 075704 (2015).

[28] L. O'Brien, M. J. Erickson, D. Spivak, H. Ambaye, R. J. Goyette, V. Lauter, P. A. Crowell, and C. Leighton, Kondo physics in non-local metallic spin transport devices, Nat. Commun. **5**, 3927 (2014).

[29] H. Idzuchi, A. Fert, and Y. Otani, Revisiting the measurement of the spin relaxation time in graphene-based devices, Phys. Rev. **91**, 241407(R) (2015).

[30] M. Furis, D. L. Smith, S. Kos, E. S. Garlid, K. S. M. Reddy, C. J. Palmstrøm, P. A. Crowell, and S. A. Crooker, Local

Hanle-effect studies of spin drift and diffusion in n:GaAs epilayers and spin-transport devices, New J. Phys. **9**, 347 (2007).

[31] T. A. Peterson, S. J. Patel, C. C. Geppert, K. D. Christie, A. Rath, D. Pennachio, M. E. Flatté, P. M. Voyles, C. J. Palmstrøm, and P. A. Crowell, Spin injection and detection up to room temperature in Heusler alloy/n-GaAs spin valves, Phys. Rev. B **94**, 235309 (2016).

[32] J. Sun, Spin-current interaction with a monodomain magnetic body: A model study, Phys. Rev. B **62**, 570 (2000).

[33] J. Z. Sun, Spin angular momentum transfer in current-perpendicular nanomagnetic junctions, IBM J. Res. Dev. **50**, 81 (2006).

[34] K. Pi, Wei Han, K. M. McCreary, A. G. Swartz, Yan Li, and R. K. Kawakami, Manipulation of Spin Transport in Graphene by Surface Chemical Doping, Phys. Rev. Lett. **104**, 187201 (2010).

[35] F. A. Chaves, D. Jiménez, A. A. Sagade, W. Kim, J. Riikonen, H. Lipsanen, and D. Neumaier, A physics-based model of gate-tunable metal-graphene contact resistance benchmarked against experimental data, 2D Mater. **2**, 025006 (2015).

[36] Z. Wang, C. Tang, R. Sachs, Y. Barlas, and J. Shi, Proximity-Induced Ferromagnetism in Graphene Revealed by the Anomalous Hall Effect, Phys. Rev. Lett. **114**, 016603 (2015).

[37] S. Singh, J. Katoch, T. Zhu, K. Y. Meng, T. Liu, J. T. Brangham, F. Yang, M. E. Flatté, and R. K. Kawakami, Strong Modulation of Spin Currents in Bilayer Graphene by Static and Fluctuating Proximity Exchange Fields, Phys. Rev. Lett. **118**, 187201 (2017).

[38] M. Cattelan, G. W. Peng, E. Cavaliere, L. Artiglia, A. Barinov, L. T. Roling, M. Favaro, I. Píš, S. Nappini, E. Magnano, F. Bondino, L. Gavioli, S. Agnoli, M. Mavrikakis, and G. Granozzi, The nature of the Fe-graphene interface at the nanometer level, Nanoscale **7**, 2450 (2015).

[39] T. Frank, M. Gmitra, and J. Fabian, Theory of electronic and spin-orbit proximity effects in graphene on Cu(111), Phys. Rev. B **93**, 155142 (2016).